TRANSMUTATION IN A GOLD–LIGHT WATER ELECTROLYSIS SYSTEM

ELECTROLYTIC DEVICES

KEYWORDS: *nuclear transmutation, isotopic abundance, crater*

TADAYOSHI OHMORI* *Hokkaido University, Catalysis Research Center*
Kitaku Sapporo 060, Japan

TADAHIKO MIZUNO *Hokkaido University, Faculty of Engineering*
Kitaku Sapporo 060, Japan

YOSHINOBU NODASAKA *Hokkaido University, School of Density*
Kitaku Sapporo 060, Japan

MICHIO ENYO *Hakodate National College of Technology*
Tokuracho Hakodate 042, Japan

Received March 31, 1997
Accepted for Publication November 4, 1997

Mercury, krypton, nickel, and iron with anomalous isotopic compositions were found to be produced on or in gold electrons during light water electrolysis. In addition, silicon and magnesium with anomalous isotopic compositions were also detected in the precipitates separated from the gold electrode electrolyzed at extremely high current densities. After the electrolysis, the surface of the electrode exhibited an extraordinary structure, i.e., a number of microcraters like volcanoes were developed. The structure of the outside wall of the craters was very much like that of the precipitates, and hexagonal crystallite layers in the inside wall of the craters suggested a partial recrystallization of the electrode material due to some intense heat evolution. The craters developed along the rim of the microcracks, microholes, and scraped edges of the electrode. These results suggest that some nuclear transmutation reactions occur during the electrolysis to produce these effects.

I. INTRODUCTION

In earlier studies[1] we reported that a considerable amount of iron atoms, much greater than the amount of impurity iron, was detected on or in a gold electrode after light water electrolysis. Subsequent studies found that the iron atoms possess an anomalous isotopic composition evidently deviating from its natural isotopic abundance, and there a linear relationship exists between the amount of iron and the excess energy produced.[2,3] Recently, by more detailed investigations,[4–6] we found the production of several elements with anomalous isotopic contents besides iron—mercury, osmium, silicon, etc. These results were supported by several researchers. Yamada et al.[7] investigated the isotopic composition of iron produced on or in a gold electrode after electrolysis in a sodium sulfate light water solution and perfectly reproduced our results. Miley and Patterson[8] and Miley et al.[9] investigated reaction products in light water electrolysis with an electrode of plastics beads covered with nickel film (Patterson-type electrode) and reported that ~40% of nickel electrode material was converted into iron, chromium, magnesium, copper, silver, etc., after the electrolysis, and the chief product, iron, occupying 15% of the product, has an isotopic composition that is very close to that of iron obtained in our study. Dash et al.[10] reported that small amounts of gold and silver were formed on a crystallographically distorted part of a palladium electrode after electrolysis in both light water and heavy water sulfuric acid solutions.

The production of elements with isotopic compositions definitely different from the natural isotopic abundance is a decisive key to confirming the occurrence of the nuclear transmutation reaction because the isotopic contents of elements should be universally constant everywhere on the earth.

In this study we tried to detect the element species with anomalous isotopic compositions on or in a gold electrode after electrolysis under various conditions. As

*E-mail: tohmori@cat.hokudai.acljp

a result, we found the production of considerable amounts of mercury, krypton, nickel, and iron and small amounts of various kinds of heavy metal elements and, in addition, an extraordinary structure on the gold electrode surface that suggests a microexplosion due to the nuclear transmutation reaction outlined in Refs. 4, 5, and 6. Contained herein is a description of the detailed results and discussion on some possible nuclear reactions that lead to the production of these elements.

II. EXPERIMENT

The electrolytic cell used was made of fused quartz in the form of a flat-bottomed cylinder (~6.2 cm in diameter × 15 cm tall) with a 5-cm-high silicone rubber stopper holding a working electrode, a counter electrode, a thermocouple, and a quartz glass inlet tube for hydrogen gas. The electrolytic cell was cleaned carefully with hot mixed acid (1:1 H_2SO_4 + HNO_3), rinsed with Milli-Q water using an ultrasonic vibrator. The working electrode was clamped on a 0.03-cm-diam gold wire coated with a thin Teflon film except for the terminal end. The cell was placed in an air thermostat regulated at 21 ± 1°C.

The working electrodes used were cold-worked gold sheets (2.5 to 5.0 cm^2 apparent area; 0.1 mm thick; 99.99% pure; Ag: 21 ppm; Pd: 3 ppm; Cu: 1 ppm; Fe, Rh, Pt, Si: <1 ppm; Hg and Os: not detected), whose surface was scraped with a cleaned glass fragment (cleaned with hot mixed acid and Milli-Q water). The roughness factor of the electrode determined from the double layer capacitance[11] was 2.0. The counter electrode was a 1 × 7 cm, 80-mesh platinum net (99.98% pure; Rh: 18 ppm; Pd, Cr, Si: 2 ppm; Cu, Fe, B, Ca: <1 ppm; Hg and Os: not detected). The working and the counter electrodes were placed at the bottom of the electrolytic cell to minimize the temperature gradient in the electrolyte solution by vigorously stirring with hydrogen and oxygen gas bubbles evolved from these electrodes.

The electrolyte solutions were 0.5 *M* sodium sulfate or 0.5 *M* sodium carbonate solution prepared from Merck sprapur reagents. The volume of the electrolyte solution was 100 ml. The contents of major impurity atoms in sodium carbonate and sodium sulfate solutions used were analyzed by inductively coupled plasma (ICP) spectroscopy. There was no essential difference in the contents of the impurity atoms between the two solutions. Here, only the result obtained in the sodium carbonate solution is shown in Fig. 1. The numbers of magnesium,iron, nickel, and mercury atoms containing 0.5 *M* sodium carbonate solution estimated from this result are only in the range from 10^{13} to 10^{14} atoms.

The electrolysis was carried out galvanostatically for 7 to 30 days at a constant current ranging from 1 to 3 A. Excess energy measurement was carried out simultaneously only in the case of the electrolysis conducted at a current of 1 A. In this case, cell voltage and increments of the electrolyte solution temperature were monitored by a recorder. Before the electrolysis, the working electrode was kept at a reversible hydrogen electrode potential by passage of hydrogen gas into the cell. During the electrolysis, Milli-Q water was added every 24 h to keep the total amount of solution constant.

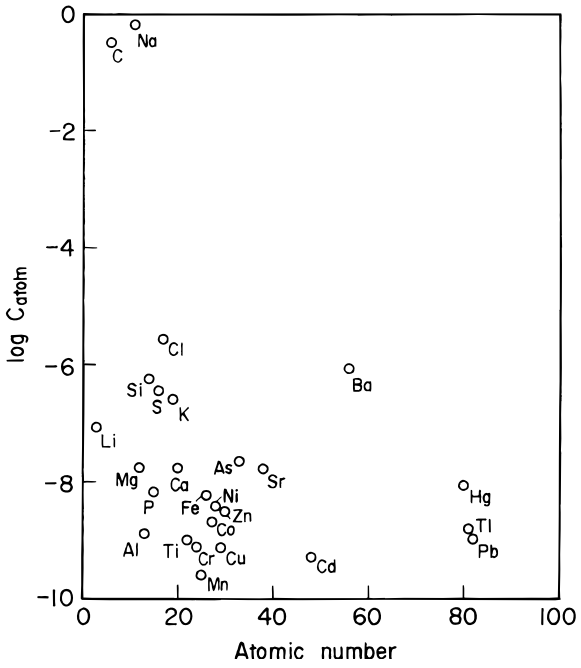

Fig. 1. Relative concentrations of elements contained in a sodium carbonate solution used as electrolyte.

In the present work, fine black porous precipitates were observed at the bottom of the electrolytic cell when electrolyzed at current densities of >200 mA/cm^2. The precipitates were collected and placed on either a nickel or silver plate of ~1 cm^2. The constituting elements on or in the electrode after the electrolysis and on or in the precipitates produced simultaneously were identified by means of Auger electron spectroscopy (AES), electron probe microanalysis (EPMA), and secondary ion mass spectrometry (SIMS), and their isotopic compositions were surveyed by means of SIMS. The AES measurement was conducted with an ANELVA AAS-200 Auger electron spectrometer with 3.0 keV of beam energy, 2.5 A of filament current, and 0.3% resolution. The SIMS measurement was carried out up to mass number 210 by O_2^+ ion irradiation (100-nA primary ion current, 12-keV accelerating voltage, and 500 resolution) with a Hitachi IMA-3 ion microanalyzer. The precision of the measurement of the isotopic composition was checked with a sample consisting of various kinds of oxides with natural isotopic components and proved to be within ±0.5% for ^{208}Pb, ^{107}Ag, ^{39}K, ^{24}Mg, ^{7}Li, and ±1% for ^{56}Fe and ^{28}Si.

The EPMA measurement was conducted using a Shimadzu EMX-SM (10.5-keV accelerating voltage, 100-nA ion current, 400-μm beam diameter, and 20-eV resolution).

In this study, the elements produced on or in the gold electrodes and their isotopic compositions were investigated with five electrode samples electrolyzed under different conditions as shown in Table I. The elements constituting the precipitates were analyzed, and their isotopic compositions were surveyed with electrodes 4 and 5, several other electrodes electrolyzed at current densities of >500 mA/cm^2, and several precipitates. Electrode 1 is the same kind as that used for iron analysis in previous studies.[4–6] The excess energy was measured with 10s electrodes in sodium sulfate and sodium carbonate solutions.

III. RESULTS AND DISCUSSION

III.A. Analysis of Elements and Their Isotopic Compositions

III.A.1. Analysis of Elements

A typical SIMS spectrum of an electrode after the electrolysis in sodium carbonate solution at a current density of 500 mA/cm^2 is shown in Fig. 2. In this spectrum, signals of Li^+, B^+, Na^+, Mg^+, Al^+, Si^+, K^+, Ca^+, Sc^+, Ti^+, Fe^+, Ni^+, Kr^+, Hg^+, Pb^+, and rare-earth element ions such as Sm^+, Eu^+, Dy^+, Er^+, Gd^+, etc. are discernible. The signals of mass numbers 82, 83, 84, and 86 can be identified as the signals of Kr^+ as will be shown later. For the spectrum of mass number 32, signals of O_2^+ and S^+ may overlap, and for the spectrum of mass numbers from 63 through 66, two or three kinds among TiO^+, S_2^+, Cu^+, and Zn^+ signals are considered to be overlapping, so the quantification of sulfur, copper, and zinc could not be achieved by SIMS measurement, although some considerable amounts of these elements are known to be present from the analysis by AES and EPMA. The source of krypton corresponding to the SIMS signals is quite inconceivable in the present electrolysis condition.

TABLE I

Electrolysis Systems Used for Element Analysis on or in the Electrode

Sample	Approximate Electrode Area (cm^2)	Solution	Current (A)	Electrolysis Time (days)
1	5	Na_2SO_4	1	7
2	2.5	Na_2SO_4	1	7
3	5	Na_2SO_4	1	7
4	2	Na_2CO_3	2	30
5	2	Na_2CO_3	3	20

The relative concentrations of the individual elements were approximately estimated from their SIMS signal intensities using the following equation:

$$C_{ion} = r \frac{I_i}{I_m} \ , \qquad (1)$$

where I_i and I_m are ion intensities of individual and total elements, respectively, present in a matrix of SIMS, and r is the relative sensitivity factor of the individual elements. In the present study, I_m was taken as constant as a rough approximation. The logarithms of the relative concentrations of elements present on or in the gold electrodes after electrolysis in sodium carbonate solutions at a current density of 500 mA/cm^2, corresponding to a depth of $\sim$0 to 180, 360 to 540, and 1080 to 1260 Å from the electrode surface, are shown in Fig. 3. It can be seen from this figure that the major elements are gold, hydrogen, carbon, oxygen, silicon, iron, krypton, and mercury. Boron, sodium, magnesium, aluminum, potassium, calcium, titanium, chromium, manganese, cobalt, nickel, rhodium, ruthenium, silver, palladium, tungsten, rhenium, osmium, platinum, lead, and several rare-earth metal elements are found to be present as minor elements. The contents of mercury, iron, and nickel, the major product elements, detected in the uppermost layers of the electrode (0 to 180 Å) were 7.3, 5.2, and 0.4%, respectively, which decreased linearly with increasing depth of the electrode. As a result, these contents in the deepest layers measured (2520 to 2700 Å) fell to 2.9, 1.9, and 0.1%, respectively. The amounts of mercury, iron, and nickel estimated from this result were 9×10^{16}, 6×10^{16}, and 5×10^{15} atoms, respectively, which are approximately three orders of magnitude larger than the total amounts of mercury, iron, and nickel contained in sodium carbonate or sodium sulfate solutions as impurities. According to the SIMS analysis of the electrode before the electrolysis conducted previously,[5] the amount of iron was nearly two orders of magnitude smaller than that produced after the electrolysis, and no mercury, nickel, or krypton was detected. Therefore, we have no choice but to search other sources for the formation of mercury, iron, and nickel other than that due to the deposition of impurities.

It is surprising that the atomic concentration of krypton reaches approximately ten times that of gold. This could mean that krypton was produced and stored in the bulk of electrode material during the electrolysis, which is partly diffused up to the outermost layer of the electrode and then released continuously as Kr^+ into the SIMS matrix by the O_2^+ irradiation during the SIMS analysis. The absence of krypton in the electrode before the electrolysis[5] confirms this view.

The presence of mercury, iron, and silicon was again confirmed by EPMA measurement. Figure 4 shows

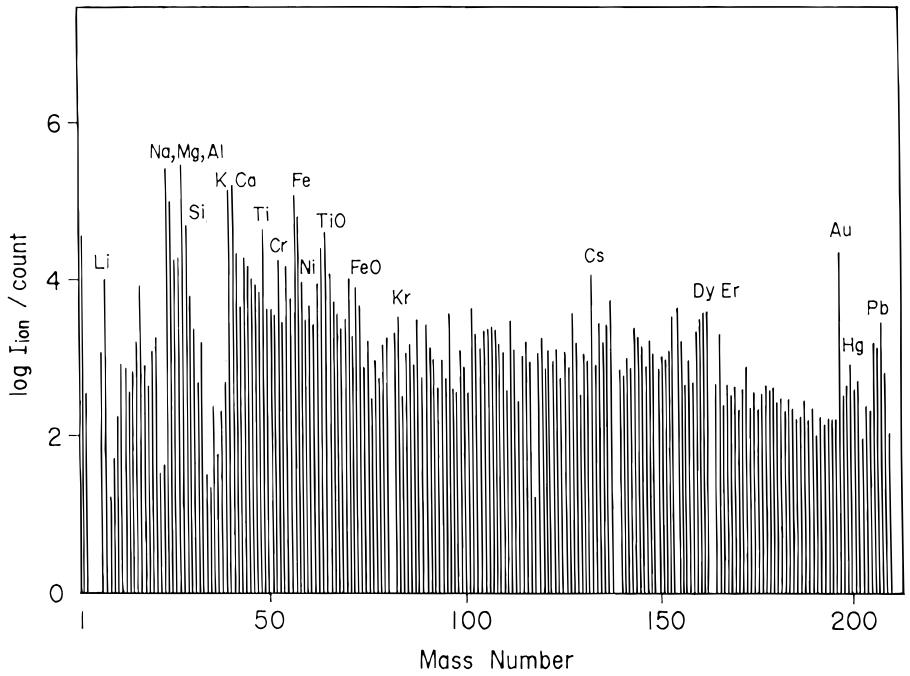

Fig. 2. SIMS spectrum in the uppermost layers of the electrode after the electrolysis in Na_2CO_3 solution at 500 mA/cm^2 (No. 4).

EPMA mapping images of the distribution of gold, mercury, iron, and silicon present on the surface of the gold electrode after the electrolysis in sodium carbonate solution at a current density of 500 mA/cm^2 (No. 4). Here, the bright spots show the presence of the elements specified. The distributions of these elements are almost uniform in spite of the nonuniformity of the surface structure of the gold electrode, as is shown later. The contents of these atoms are in the order Si $<$ Fe $<$ Hg, being estimated at $\sim$1 to 10% in view of the moderate sensitivity of EPMA. This estimation is consistent with that by AES and SIMS analyses.

III.A.2. Isotopic Composition

The isotopic composition of the major product elements—mercury, nickel, iron, and krypton—showed significant deviations from their natural values. Besides these elements, various kinds of minor product elements—osmium, rhenium, tungsten, ruthenium, and several rare-earth elements—showed significant deviations. On the other hand, lead, silver, and elements lighter than iron scarcely showed such deviations. In what follows, we will show the isotopic composition deviations for mercury, nickel, iron, and krypton in detail.

III.A.2.a. Mercury. Figure 5 shows the isotopic compositions of mercury plotted against the depth from the electrode surface for two electrodes (Nos. 4 and 5) after electrolysis in sodium carbonate solutions. Figure 5 shows that the deviations of the isotopic composition of mercury from the natural values are clearly discernible, and in both cases, there is a common characteristic in the manner of the deviation; i.e., ^{200}Hg is much higher than its natural isotopic abundance level, while ^{202}Hg, the maximal isotopic component in nature, is lowered significantly. Thus ^{200}Hg is 36% (1800 to 2700 Å) to 28% (0 to 180 Å) for electrode 4 and 55% for electrode 5, becoming the maximal isotopic component. No noticeable differences can be mentioned for other isotopes. In several isotopes, the isotopic composition changes to some extent with the depth of the electrode, but any common tendencies are not perceived between electrodes 4 and 5. The unequivocal deviation of the isotopic composition of ^{200}Hg and ^{202}Hg from the natural one shown in this figure indicates that mercury was produced by some nuclear transmutation reaction.

III.A.2.b. Nickel. The isotopic composition of nickel detected on or in electrode 5 is shown in Fig. 6. The contents of ^{60}Ni and ^{61}Ni increase significantly with increasing depth of the electrode. On the other hand, the major component in nature, ^{58}Ni, decreases. Note that the contents of these isotopes are close to the natural isotopic abundance in the outermost layers of the electrode. According to the result of the SIMS analysis, the amount of nickel present on or in the electrode can be estimated at $\sim 5 \times 10^{15}$ atoms, which is much smaller than the amounts of mercury and iron but much larger than the total amount of nickel impurity in the solution (Fig. 1). Therefore, it would be natural to consider that nickel atoms detected here are the product of some nuclear transmutation reaction.

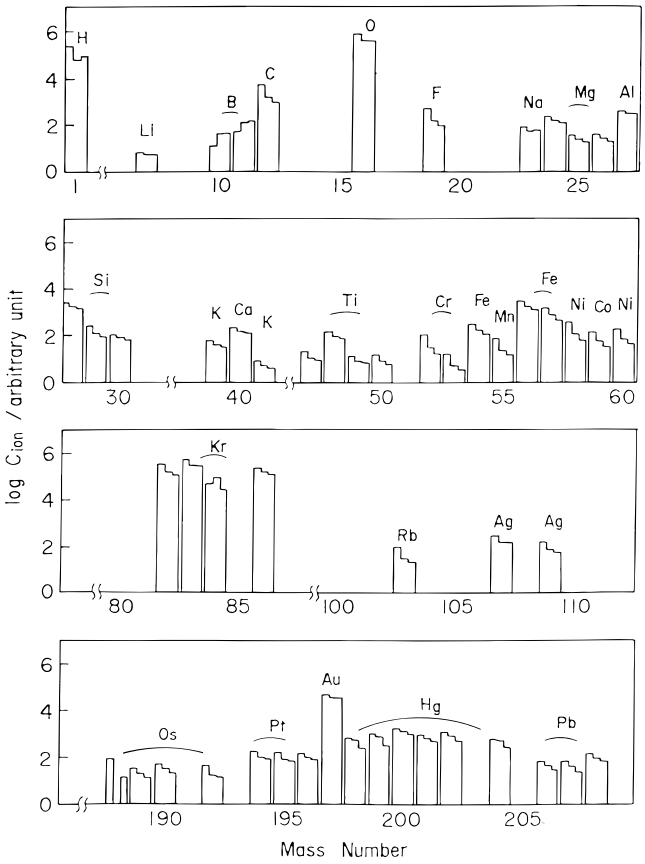

Fig. 3. Relative concentration of elements present on or in the gold electrode after electrolysis in Na_2CO_3 solutions at 500 mA/cm^2 (No. 4). The left, center, and right levels of the individual bars correspond to the values of layers 1 through 180 (outermost), 360 through 540, and 1080 through 1260, respectively. The ordinate is given in log units.

III.A.2.c. Iron. As reported in previous papers,[2,3] we have already observed an increase in the content of ^{57}Fe for iron present on or in the gold electrode after electrolysis in sodium sulfate solution at a current density of 100 mA/cm^2 (No. 1). The isotopic contents of iron obtained for electrodes 2 through 5 are listed in Table II together with that for electrode 1. Similar results were obtained for electrodes 3 and 4. For electrodes 2 and 5, the contents of ^{57}Fe are approximately half of those obtained for electrodes 3 and 4. However, in every case, the contents of ^{57}Fe exceeded by 4 to 13 times its natural isotopic abundance. The contents of ^{54}Fe did not deviate much from its natural value. In this context, one can see that the isotopic deviation of iron observed in the present study well reproduces the result in the previous one. The degree of the isotopic deviation of iron seems to be independent of the nature of the electrolyte used. The isotopic compositions of iron are compared with the depth of the electrode for different electrolysis conditions in Fig. 7 (Nos. 2 and 4). For electrode 2, Fig. 7a, the distributions of ^{54}Fe, ^{56}Fe, and ^{57}Fe are nearly constant, independent of the depth from the electrode surface. Essentially the same results were obtained for electrodes 3 and 5. On the other hand, for electrode 4, Fig. 7b, the content of ^{57}Fe is highest (^{56}Fe, lowest) at the outermost layers of the electrode. For electrode 1, ^{57}Fe was lowest at the outermost layers.[2,3]

To check the possibility of the overlap of $^{56}FeH^+$ in the ^{57}Fe signals, the signal intensity ratios of mass 57 to mass 56 and of mass 73 to mass 72, corresponding to the signals of $^{57}FeO^+$ and $^{56}FeO^+$, are plotted against the depth of the electrode for electrodes 2 and 4 in Fig. 8. For electrode 4, Fig. 8b, the plots were limited within a depth of 720 Å because of a large scattering of plots owing to the small signal intensities of mass numbers 72 and 73. These figures show that the plots of $^{57}Fe/^{56}Fe$ and $^{57}FeO/^{56}FeO$ are very close to each other. Hence, we can regard the signals of mass 57 for electrodes 2 and 4 as the signals of $^{57}Fe^+$. From these results, there is no doubt that $\sim 6 \times 10^{16}$ atoms of iron with definitely different isotopic composition from natural values were produced by some nuclear transmutation reaction.

The amounts of excess energy evolved on 10s electrodes in electrolysis at current densities of 100 to 200 mA/cm^2 were in the range of 0.5 to 1 W. These values coincide with those obtained in previous work.[3] However, under electrolysis at $>$200 mA/cm^2, where a considerable amount of precipitates was produced, any linear relationships between the excess energy and the amount of produced iron, which were observed in electrolysis at 100 to 200 mA/cm^2, were not observed. This result may be acceptable in view of the production of considerable amounts of mercury, nickel, and krypton and small amounts of other various heavy metal elements in the present electrolysis.

III.A.2.d. Krypton and Other Inert Gases. As seen from Fig. 2, there are several noticeable signals in the mass number region of krypton (82, 83, 84, and 86). To check whether they give the signals of Kr^+ exclusively, the variations of these signal intensities were plotted against the depth of the electrode (Fig. 9). As seen from this figure, the intensities of these signals decreased nearly in parallel with each other with increasing depth. This indicates that the ion species giving these signals are identical, i.e., Kr^+. Figure 10 shows the isotopic composition of krypton on or in the electrode after electrolysis (No. 5). The isotopic composition of krypton is also quite different from its natural one. The content of ^{82}Kr, 68%, is remarkably higher than its natural value of 11.56%. Other components are lower than their natural ones.

Other inert gases such as helium, neon, argon, and xenon might have been produced through some nuclear transmutation processes in view of the stability of these nuclei. However, it is impossible to detect helium by SIMS because of its extremely low sensitivity. Neon and argon were not identified because of the overlap with Ca^{2+} and

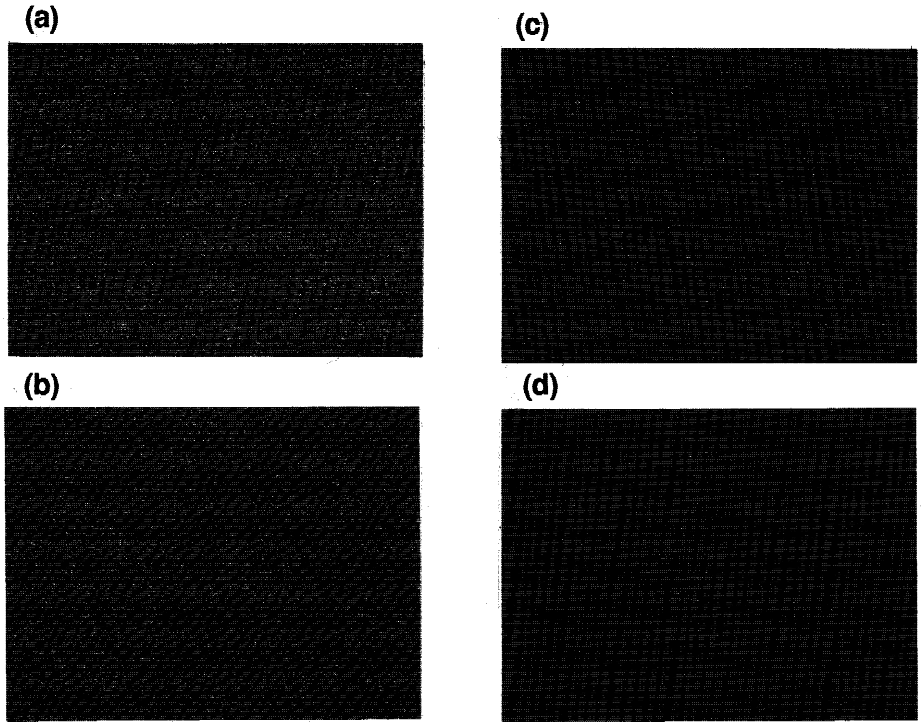

Fig. 4. EPMA images of (a) Au, (b) Hg, (c) Fe, and (d) Si on the electrode after the electrolysis in Na_2CO_3 solution at 500 mA/cm^2 (No. 4). Wavelengths of the specific X ray are 1.276, 1.240, 1.937, and 7.126 Å for Au, Hg, Fe, and Si, respectively. The SEM images in Fig. 18 correspond to the surface structure of the electrode.

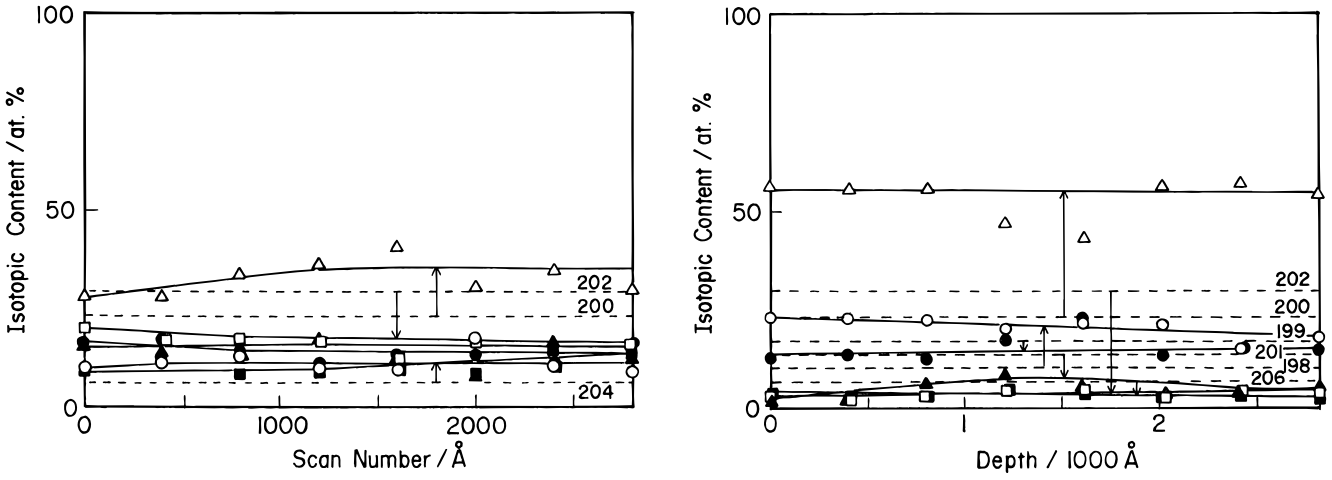

Fig. 5. Isotopic compositions of Hg present on or in the electrodes after electrolysis in Na_2CO_3 at (a) 500 mA/cm^2 (No. 4) and (b) 750 mA/cm^2 (No. 5): ○ = ^{198}Hg, ● = ^{199}Hg, △ = ^{200}Hg, ▲ = ^{201}Hg, □ = ^{202}Hg, and ■ = ^{204}Hg. Broken lines show natural isotopic abundance levels.

Ca^+ signals, respectively. The signal intensities corresponding to xenon (mass numbers 129, 130, 131, 134, and 136) were much weaker than those of krypton. This result contrasts with that in heavy water electrolysis with a palladium electrode,[12,13] suggesting that the nuclear transmutation reactions occurred on or in a gold electrode are essentially different from those occurring on or in the palladium electrode.

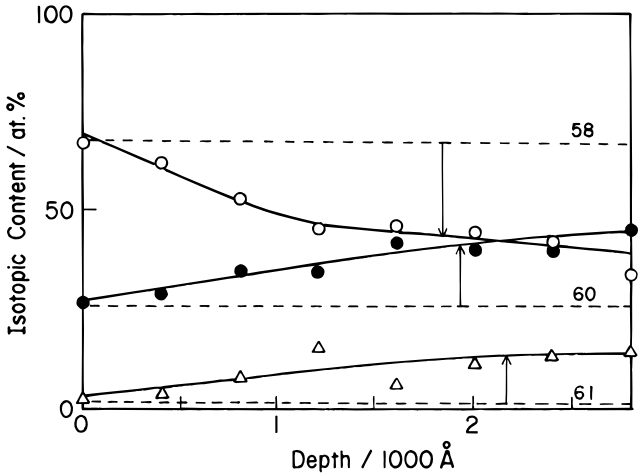

Fig. 6. Isotopic composition of Ni present on or in the electrode after electrolysis in Na_2CO_3 at 750 mA/cm^2 (No. 5): ○ = ^{58}Ni, ● = ^{60}Ni, and △ = ^{61}Ni.

TABLE II

Isotopic Contents of Fe Produced in Various Electrolysis Systems

Sample	Total Ion Intensity (count)	Isotopic Content (%)		
		^{54}Fe	^{56}Fe	^{57}Fe
1	17 205	3.2	74.7	22.0
2	619 950	5.6	84.7	9.6
3	192 134	3.7	67.4	28.9
4	1 254 164	7.0	67.6	25.3
5	141 211	6.6	84.1	9.2
Natural value		5.82	91.66	2.19

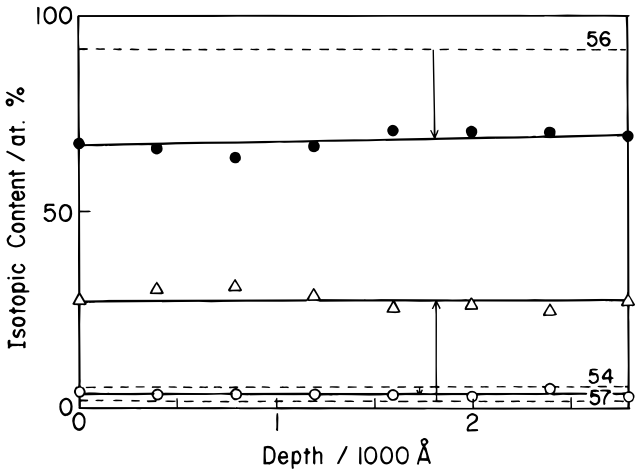

(a)

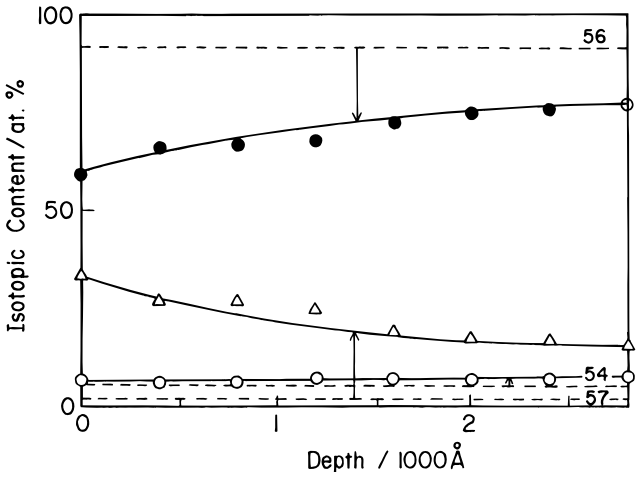

(b)

Fig. 7. Isotopic composition of Fe present on or in the electrode after electrolysis in (a) Na_2SO_4 at 200 mA/cm^2 (No. 2) and (b) Na_2CO_3 at 500 mA/cm^2 (No. 4); ○ = ^{54}Fe, ● = ^{56}Fe, and △ = ^{57}Fe.

III.A.2.e. Other Elements. Lead, silver, and elements lighter than iron present on or in the electrode showed the isotopic compositions close to their natural isotopic abundance. The isotopic compositions of these elements are listed in Table III together with their natural values. This shows that these elements are mostly impurities. The fact that there are no product elements from any nuclear reaction in the elements lighter than iron inevitably leads to the conclusion that mercury, krypton, nickel, iron, and other heavy metal elements with anomalous isotopic compositions are not produced by any nuclear fusion reaction starting from the interaction among hydrogen and hydrogen, hydrogen and deuterium, deuterium or hydrogen and tritium, etc., proposed so far, but they are produced by some nuclear interactions of a completely different type associated with heavy elements. It would be most reasonable to consider that the starting elements are hydrogen (or proton) and gold of the electrode material, which has already been proposed by Miley and Patterson,[8] Miley et al.,[9] and ourselves.[4–6]

In every electrode small amounts of lead and titanium were detected. The amounts of lead and titanium were estimated at $\sim\frac{1}{500}$ of the amount of gold, which, however, seems to be too high to be regarded as impurities coming from the electrolyte because both elements were contained only slightly in sodium sulfate and sodium carbonate solutions (Fig. 1). Hence, one can consider that lead and titanium are also produced by some nuclear transmutation reaction. As will be discussed in Sec. III.B, it could be assumed that titanium is produced in the form of halo atoms as an intermediate species to produce iron.

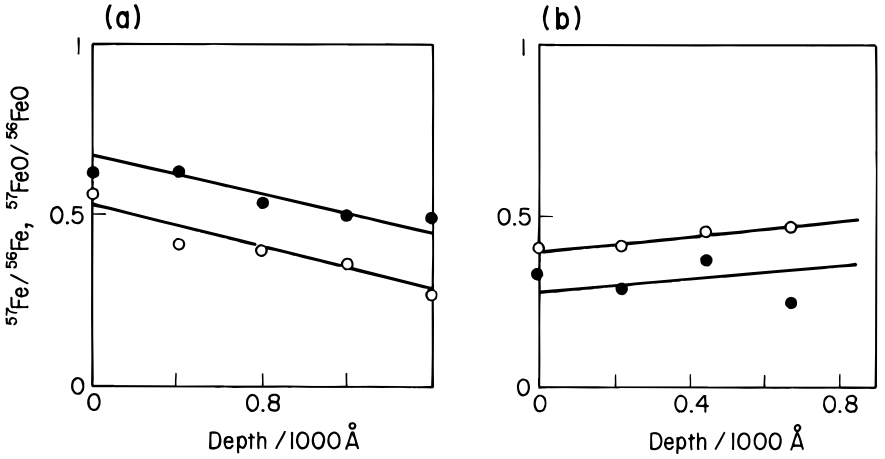

Fig. 8. Signal intensity ratio of mass number 57 to mass number 56 (○) and of mass number 72 to mass number 73 (●): (a) Na_2SO_4 at 200 mA/cm^2 (No. 2) and (b) Na_2CO_3 at 500 mA/cm^2 (No. 4).

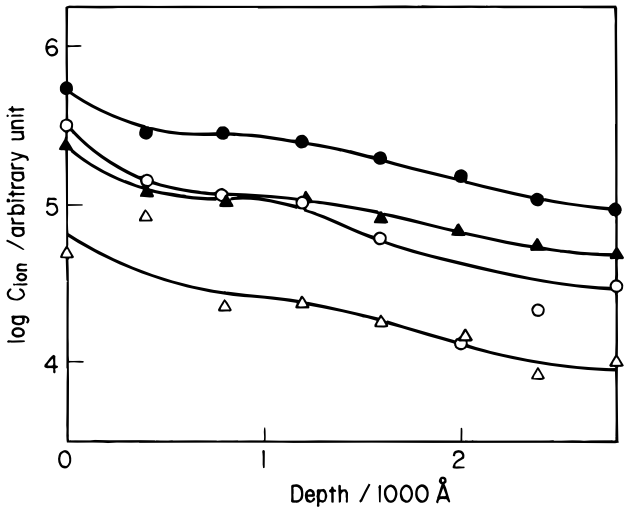

Fig. 9. Variation of signal intensities of mass numbers 82, 83, 84, and 86 corresponding to Kr against the depth of the electrode after electrolysis in Na_2CO_3 at 500 mA/cm^2 (No. 4); ○ = 82, ● = 83, △ = 84, and ▲ = 86.

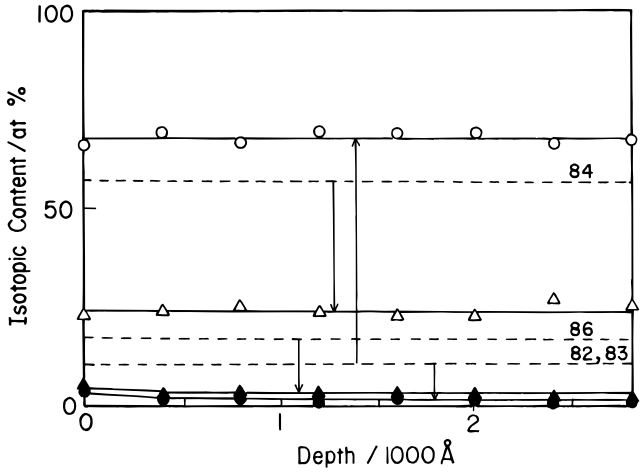

Fig. 10. Isotopic composition of Kr on or in the electrode after electrolysis in Na_2CO_3 at 750 mA/cm^2 (No. 5). Symbols correspond to those in Fig. 9.

III.B. Precipitates

A considerable amount of fine black precipitates was found to be produced at the bottom of the electrolytic cell when electrolysis was carried out in sodium sulfate or sodium carbonate solution at current densities of >200 mA/cm^2. In most cases, the precipitates began to appear 2 to 3 days after the electrolysis and gradually increased. The yield of the precipitates is in the range from 0.1 to 1 mg and seems to be different, depending on a slight difference in the manner of the surface pretreatment of the electrode. The appearance of the precipitates and their scanning electron microscopy (SEM) image are shown in Fig. 11. To all appearances, the precipitates look like fine black powder, but, in fact, they are very porous and have a number of fine porosities as shown in Fig. 11b.

Figure 12 shows AES spectra of the outermost layer of the precipitates obtained after electrolysis in sodium carbonate solution at a current density of 500 mA/cm^2. A mercury signal is visible together with platinum and gold ones. However, in the bulk of the precipitates the mercury signal disappears. Such a mercury signal was also observed in the precipitates obtained by electrolysis in sodium sulfate solutions.

Typical EPMA images of the precipitates obtained by electrolysis in sodium sulfate solution for 30 days at a current density of 750 mA/cm^2 (sample 5) are shown in Fig. 13. In this case, fairly clear mercury, platinum, and

TABLE III

Isotopic Contents of the Light Elements Present on the Surface of Various Electrodes After Electrolysis*

Element	Isotopic Content (%)					Natural Isotopic Abundance (%)
	Sample 1	Sample 2	Sample 3	Sample 4	Sample 5	
^{6}Li		8.3	8.1	7.9	7.4	7.4
^{7}Li		91.7	91.9	92.1	92.6	92.6
^{10}B	22.0	21.0	21.2	21.7	21.0	19.2
^{11}B	78.0	79.0	78.8	78.3	79.0	80.8
^{24}Mg	77.6	75.1	77.8	75.7	77.0	78.6
^{25}Mg	10.9	12.1	10.7	11.8	11.0	10.1
^{26}Mg	11.5	12.9	11.5	12.5	12.1	11.2
^{28}Si	89.8	90.5	90.6	89.5	90.1	92.2
^{29}Si	5.6	5.8	5.8	6.5	6.1	4.7
^{30}Si	4.6	3.7	3.5	4.0	3.8	3.1
^{39}K	93.2	89.6	83.1	89.0	90.3	93.1
^{41}K	6.8	10.4	16.9	11.0	9.7	6.9
^{40}Ca	96.3	95.4	95.9	95.4	94.7	96.9
^{42}Ca	0.7	1.5	1.2	1.5	2.2	0.6
^{47}Ti	7.5	8.9	8.7	9.7	8.6	7.5
^{48}Ti	74.1	70.4	71.2	69.5	70.7	74.0
^{49}Ti	5.2	6.4	6.2	6.3	6.3	5.5
^{50}Ti	5.1	6.3	5.9	6.5	6.2	5.3
^{52}Cr	83.2	79.6	77.5	80.1	81.1	83.8
^{53}Cr	9.8	13.7	15.8	13.2	12.1	9.6
^{206}Pb				25.7	27.8	25
^{207}Pb				22.8	22.6	22
^{208}Pb				50.0	48.1	52

*In these calculations, the contents of ^{46}Ti, ^{50}Cr, and ^{54}Cr are taken to be equivalent to the natural values because estimation is impossible due to their overlapping with $^{23}Na_2^+$, $^{50}Ti^+$, and $^{54}Fe^+$, respectively.

osmium images were observed together with the strongest gold image. Iron image was also observed, although it was weaker than those of the other elements. The fact that the chief component of the precipitates was gold indicates that the precipitates were separated from the gold electrode.

The isotopic composition of iron and mercury in the precipitates obtained by electrolysis in sodium carbonate solution at a current density of 500 mA/cm^2 is shown in Figs. 14 and 15, respectively. For both elements, the isotopic distribution profiles are qualitatively like those contained on or in the gold electrode after electrolysis (Figs. 4 and 6). However, the content of ^{57}Fe in iron contained in the precipitates is much greater than that contained on or in the electrode, exceeding 50% at the outermost layers of the precipitates.

Silicon and magnesium in the precipitates, different from those on or in the electrode, showed an interesting isotopic deviation. Thus, the isotopic composition of silicon in the precipitates, which is obtained by electrolysis at a current density of $<$500 mA/cm^2, is very close to the natural one, but it begins to deviate when electrolyzed at $>$500 mA/cm^2 and the extent increases with increasing current density. As a result, when electrolyzed at 1 A/cm^2, the content of ^{28}Si fell to 58%, whereas ^{29}Si and ^{30}Si rose to 25 and 17%, respectively, at the outermost layers of the electrode in sodium carbonate solution, as shown in Fig. 16. Similar results were obtained in the sodium sulfate solution. The content of silicon in the precipitates also increased significantly with increasing current density. Similar results were observed for magnesium. For magnesium, the extent of the deviation was much smaller than silicon in most cases. However, fairly large deviations were observed in a few samples. A typical example is shown in Fig. 17. These results show that the nuclear transmutation reaction to produce silicon and magnesium begins only under extremely strong electrolysis conditions.

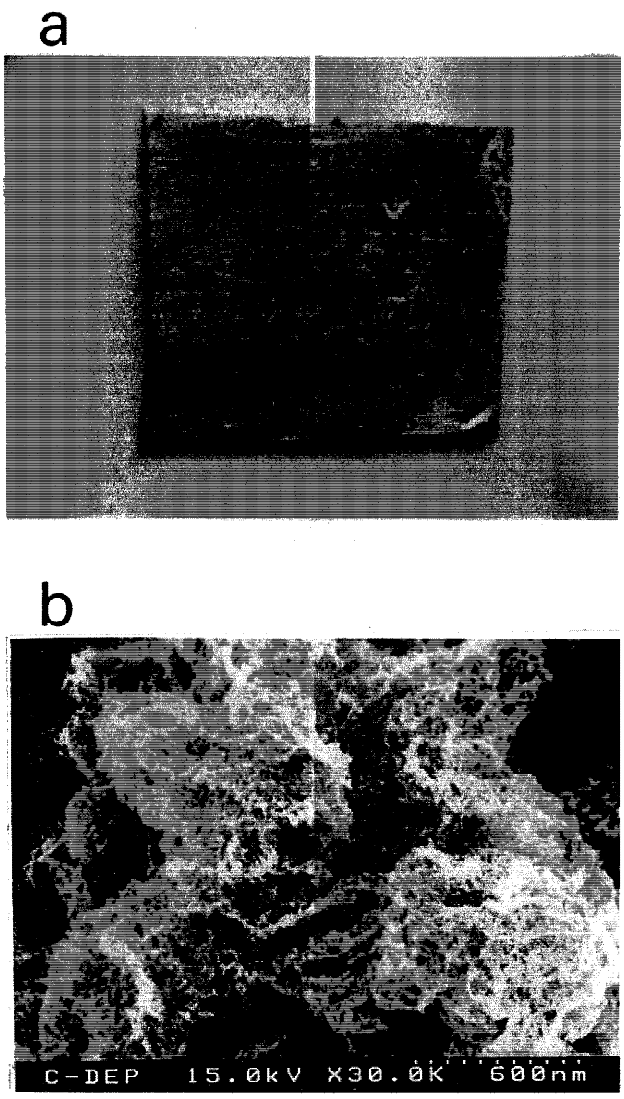

Fig. 11. (a) Precipitates placed on a Ni plate (dark part on the right side) and (b) their SEM image (×30 000).

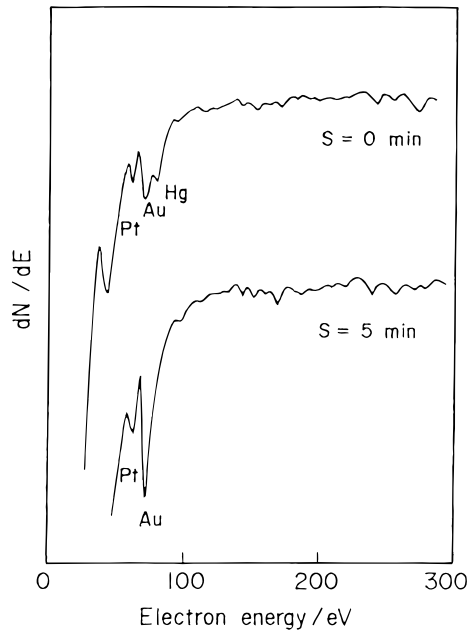

Fig. 12. Typical AES spectra of the electrode after electrolysis in K_2CO_3 at 500 mA/cm^2 (No. 4), the outermost layer, and the layer exposed after sputtering 5 min.

III.C. Surface Structure of the Electrode After the Electrolysis

The electrode surface after electrolysis at current densities of >200 mA/cm^2 exhibits a very anomalous structure. Figure 18 shows the typical SEM images of the electrode surface before and after electrolysis in sodium carbonate solution at 500 mA/cm^2 for 30 days. Many stripes, microholes, and cracks are seen on the surface of the electrode before electrolysis, which are caused by scraping with a glass fragment (Fig. 18a). To our surprise, a number of craters with various sizes developed along the stripes on the electrode surface after electrolysis (Figs. 18d and 18e). Each crater has a deep hole and very developed rim, reminding us of a volcano. The largest crater is ~20 μm in diameter and 30 μm high (Figs. 18b and 18c). From the appearance of these craters, one can imagine that some microexplosion occurred at those places and as a result, distinct craters developed just as in volcanoes. The outside wall of the craters consists of a fine porous substance, the surface of which is very like that of the precipitates. As mentioned already, the major constituent element of the precipitates is gold. Therefore, these is no doubt that these precipitates spewed out from these craters like volcanic ashes as a result of some microexplosion probably caused by some nuclear transmutation reactions.

The inside wall of the craters consists of at least three kinds of layers as observed in the magnified picture of the inner part of the crater (Fig. 18f). At the bottom the wall is made of relatively large crystallite on the order of several microns. At the intermediate part, the wall consists of more fine crystallite on the order of several hundred nanometres. The magnified picture of this layer shows that these crystallites have a hexagonal or rhombic shape assignable to Au(111) (Fig. 18g). On the outside, the wall consists of very fine crystallites of <30 nm (Fig. 18h). These crystallites also appear hexagonal, although the outline of these crystallites is not necessarily clear. Hence, these crystallites may be produced by the reconstruction of gold polycrystals of the electrode material owing to the intense heat evolved locally as a result of the microexplosion. Figure 19 shows the SEM images of the initial stages of the development of the craters. From this figure, we can clearly see that

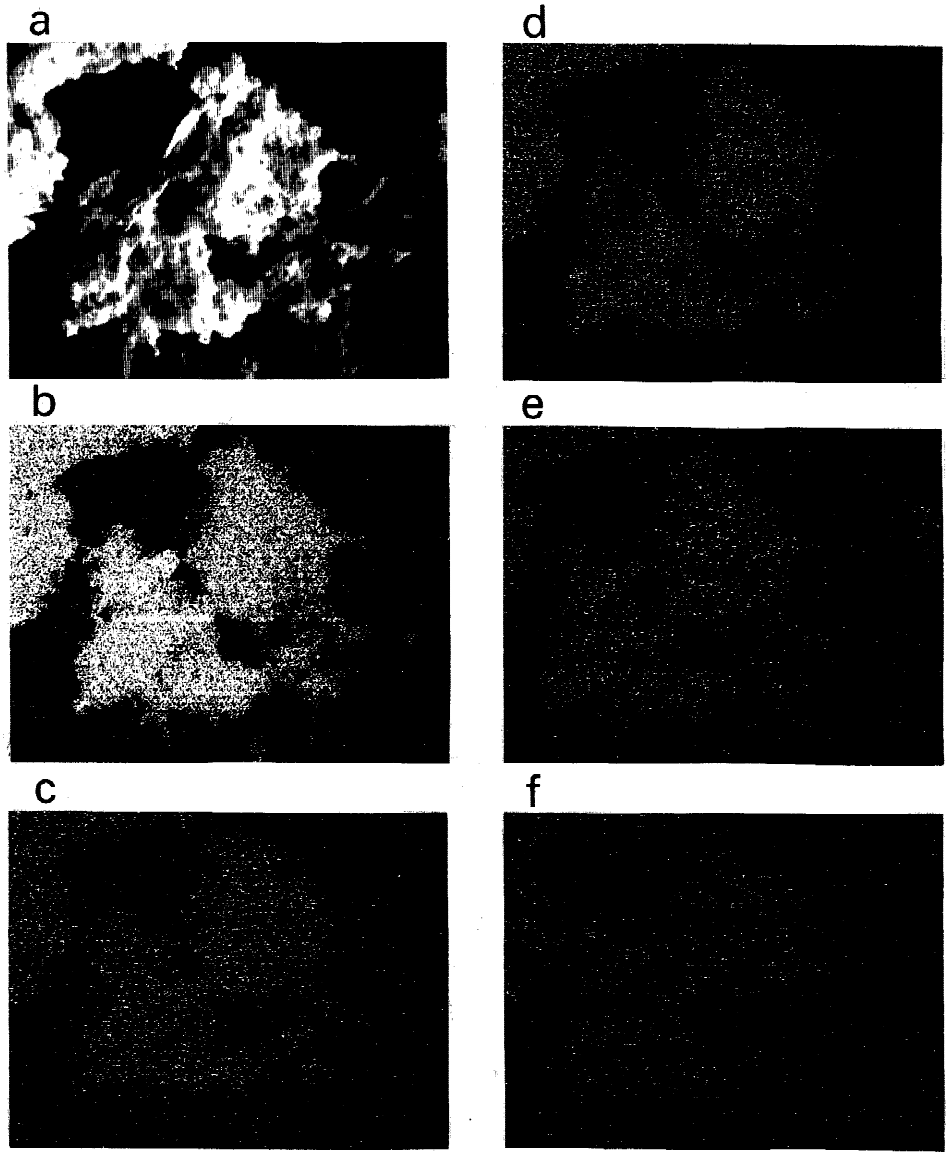

Fig. 13. The SEM and EPMA images of Au, Hg, Pt, Os, and Fe on the precipitates obtained after electrolysis in K_2CO_3 solution at 750 mA/cm^2 (No. 5): (a) SEM image (×476) and (b) through (f) EPMA images of Au, Hg, Pt, Os, and Fe, respectively. Wavelengths of the specific X rays are 1.276, 1.240, 1.313, 3.6753, and 7.126 Å for Au, Hg, Pt, Os, and Fe, respectively.

process. First, fine crystallites such as that shown in Fig. 18h form along the rim of the microholes and cracks (Fig. 19a), which pile up in a circular fashion (Fig. 19b), and thus the foundation of the craters is complete (Fig. 19c).

The transmutation reaction is expected to occur at the wall of the microholes and microcracks present on the electrode before electrolysis. Because of the nuclear transmutation reaction, infinitesimal gold particles are spewed out of the craters with intense heat evolution, recrystallizing and forming fine hexagonal crystallites. Thus, the craters are thought to develop while creating the hexagonal or rhombic crystallite wall around the reaction zone.

So far, two reports have been published on the microcrater formation related to the nuclear reaction. Numata et al.[14] found a craterlike structure on a palladium electrode after electrolysis in a LiOD heavy water solution, which is very like that shown in Fig. 19. Matsumoto[15] reported the microcrater formation on a nickel electrode in potassium carbonate solution. However, when we inspected the figure containing the craters he obtained, there was no similarity of shape and constitution to the craters we obtained. In Ref. 15 there

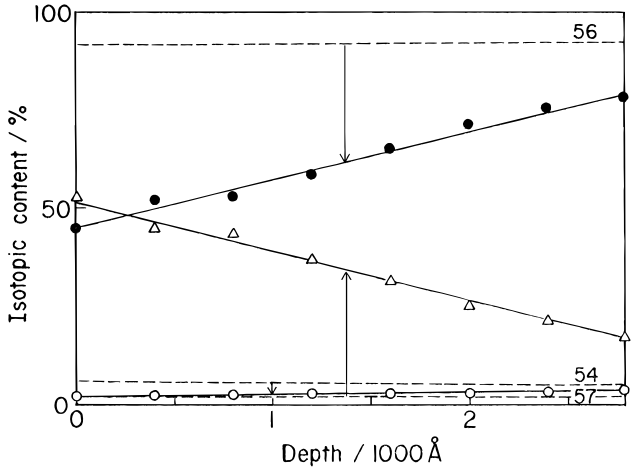

Fig. 14. Isotopic composition of Fe in the precipitates after electrolysis in Na_2CO_3 at 500 mA/cm^2: ○ = ^{54}Fe, ● = ^{55}Fe, and △ = ^{57}Fe.

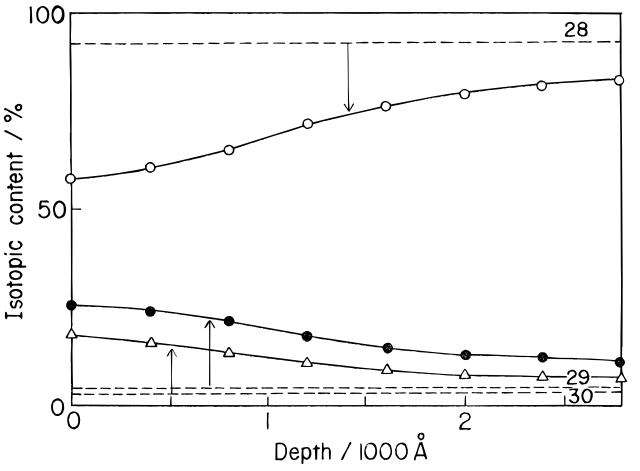

Fig. 16. Isotopic composition of Si in the precipitates after electrolysis in Na_2CO_3 at 1 A/cm^2: ○ = ^{28}Si, ● = ^{29}Si, and △ = ^{30}Si.

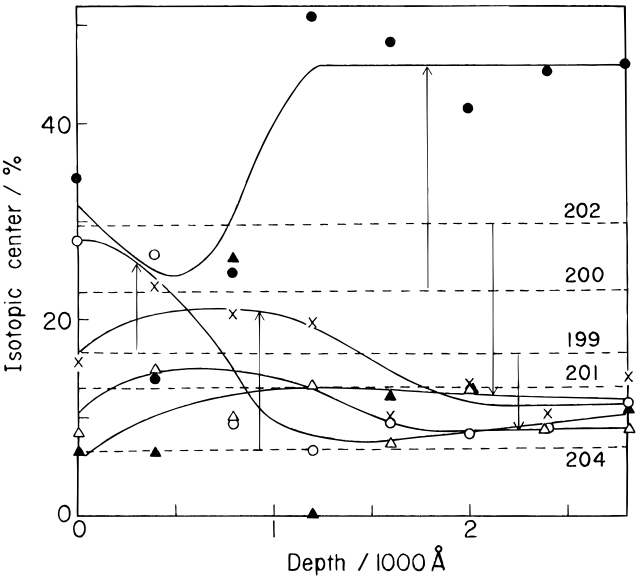

Fig. 15. Isotopic composition of Hg in the precipitates after electrolysis in Na_2CO_3 at 500 mA/cm^2: ○ = ^{199}Hg, ● = ^{200}Hg, △ = ^{201}Hg, ▲ = ^{202}Hg, and □ = ^{204}Hg. In this calculation, the content of ^{198}Hg was taken to be equal to natural isotopic abundance because the overlapping with ^{198}Pt was not neglected in this case.

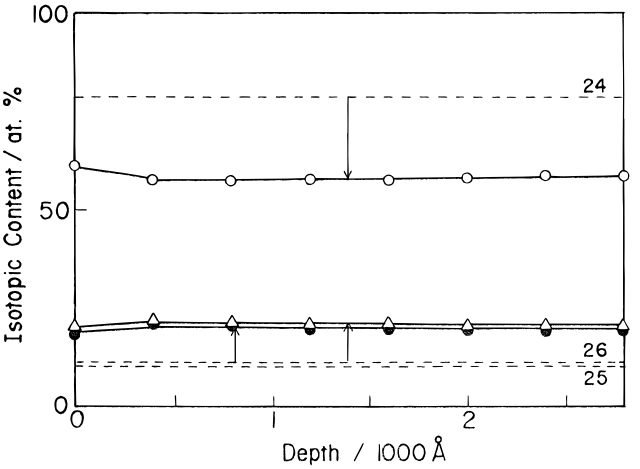

Fig. 17. Isotopic composition of Mg in the precipitates after electrolysis in Na_2CO_3 at 1 A/cm^2: ○ = ^{24}Mg, ● = ^{25}Mg, and △ = ^{26}Mg.

is little other unambiguous evidence to support the occurrence of some nuclear reaction; hence, it remains uncertain whether these craters were formed by a nuclear reaction.

III.D. Possible Transmutation Reactions

The major elements with anomalous isotopic composition present on or in the gold electrode and the precipitates were mercury, krypton, nickel, iron, and, occasionally, silicon and magnesium. In addition, osmium, tungsten, rhenium, and some rare-earth elements were found as minor products in the precipitates. In the mass number range less than iron, no anomalous elements were found on or in the electrode after the electrolysis and precipitates, although considerable amounts of anomalous silicon and magnesium were found in the precipitates produced under an extremely strong electrolysis condition. Therefore, all of the transmutation reactions that occurred in the present electrolysis are considered to have been initiated by the interaction between hydrogen or proton and gold of the electrode material. The gold-hydrogen (or gold-proton) complex thus

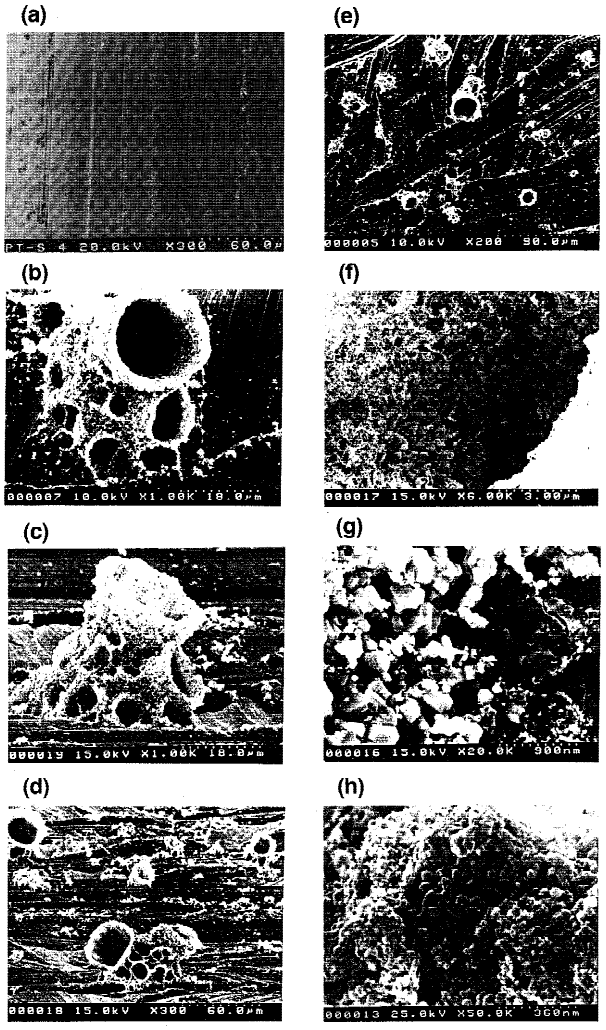

Fig. 18. The SEM images of the craters developed during electrolysis in Na_2CO_3 at 500 mA/cm^2 (No. 4): (a) electrode surface before electrolysis, (b) through (e) appearance of the craters and their distribution conditions, and (f), (g), and (h) structures of the inner part of the crater. Magnifying powers of the individual pictures are shown at the bottom of the pictures.

produced, ^{197}Au-nH (or ^{197}Au-np), would be immediately converted into mercury on the one hand or into a little lighter elements like osmium, rhenium, etc., by some fission reactions on the other. From this point of view, we can assume the following reaction schemes:

$$^{197}\text{Au} + n\text{H} \rightarrow {}^{197}\text{Au-}n\text{H} \ , \qquad (2)$$

$$^{197}\text{Au-}n\text{H} \rightarrow {}^{197+n}\text{Hg} + n\beta^- \ , \qquad (3)$$

$$^{197}\text{Au-}n\text{H} \rightarrow {}^{189+n}\text{Re} + 2{}^4\text{He} \ , \qquad (4)$$

$$\rightarrow {}^{189+n}\text{Os} + \beta^- \ . \qquad (5)$$

The production of Kr, Ni, and Fe is also considered to be caused by some fission reactions starting from

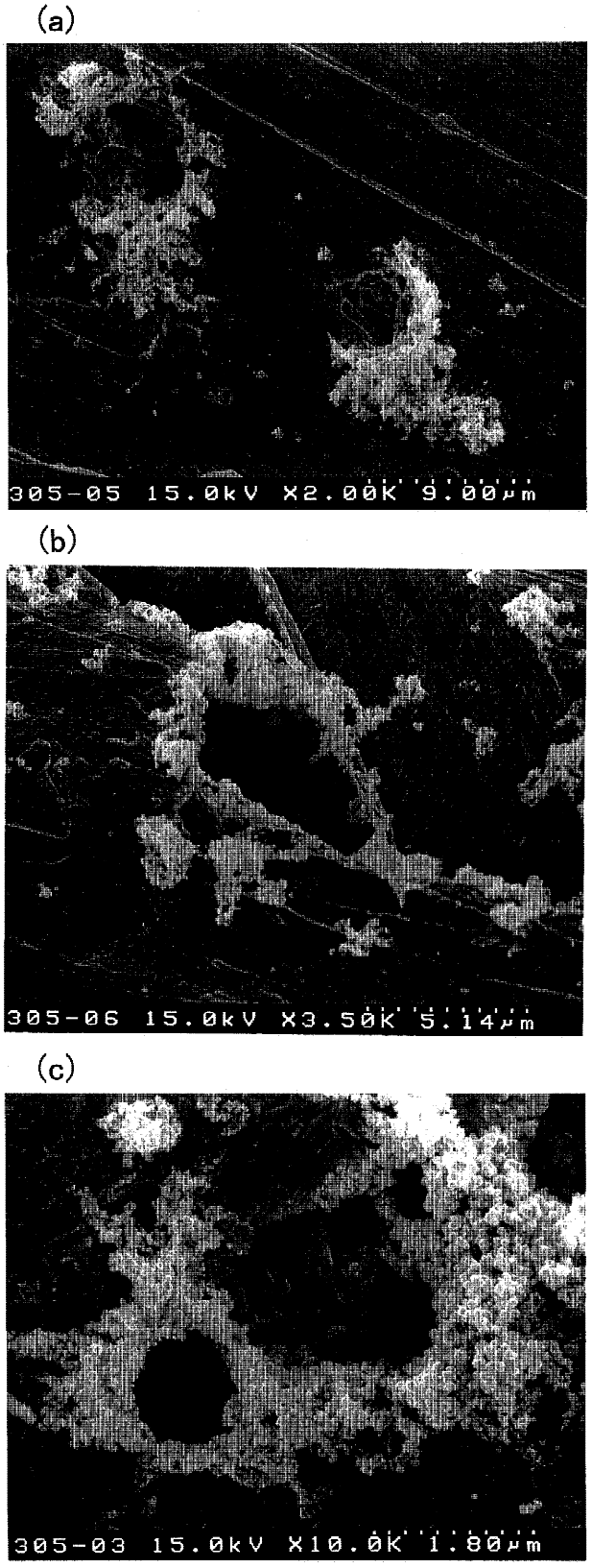

Fig. 19. The SEM images of the initial stage of crater development obtained by electrolysis in Na_2SO_4 for 30 days at 200 mA/cm^2.

^{197}Au-nH. Some examples of the assumable reactions are as follows:

$$^{197}\text{Au-H} \rightarrow {}^{86}\text{Br} + 2{}^{56}\text{Ti} \rightarrow {}^{86}\text{Kr} + 2{}^{56}\text{Fe} + 9\beta^- \ , \quad (6)$$

$$^{197}\text{Au-2H} \rightarrow {}^{86}\text{Br} + {}^{56}\text{Ti} + {}^{57}\text{Ti} \rightarrow {}^{86}\text{Kr} + {}^{56}\text{Fe} + {}^{57}\text{Fe} + 9\beta^- \ , \quad (7)$$

$$^{197}\text{Au-2H} \rightarrow {}^{84}\text{Br} + {}^{57}\text{Ti} + {}^{58}\text{Ti} \rightarrow {}^{84}\text{Kr} + {}^{57}\text{Fe} + {}^{58}\text{Ni} + 11\beta^- \ , \quad (8)$$

and

$$^{197}\text{Au-4H} \rightarrow {}^{82}\text{Br} + {}^{59}\text{Ti} + {}^{60}\text{Ti} \rightarrow {}^{82}\text{Kr} + {}^{59}\text{Co} + {}^{60}\text{Ni} + 12\beta^- \ , \quad (9)$$

where $^{56-60}$Ti atoms can be regarded as a kind of halo atom with one or several neutrons present in orbit (the same concept as an electron orbit), which has been confirmed for several light elements in the past decade.[16] These atoms are very unstable and immediately disintegrate to produce stable iron, nickel, and cobalt. A part of the halo titanium produced would release neutrons to form stable titanium atoms, which were detected in every electrode after the electrolysis and in every precipitate. In fact, for titanium present on or in the electrode after the electrolysis, a slight nonnegligible isotopic deviation from the natural value is visible in Table III, which may be caused by this reaction. Inside the craters the halo titanium atoms produced by the electrolysis at an extremely high current density would further disintegrate to produce silicon and magnesium, for example, by the following reactions:

$$^{56}\text{Ti} \rightarrow {}^{30}\text{Si} + {}^{26}\text{Mg} + 4\beta^- \ , \quad (10)$$

$$^{54}\text{Ti} \rightarrow {}^{29}\text{Si} + {}^{25}\text{Mg} + 4\beta^- \ , \quad (11)$$

$$^{56}\text{Ti} \rightarrow 2{}^{28}\text{Al} + 4\beta^- \rightarrow 2{}^{28}\text{Si} + 2\beta^- \ , \quad (12)$$

$$^{57}\text{Ti} \rightarrow {}^{28}\text{Al} + {}^{29}\text{Al} + 4\beta^- \rightarrow {}^{28}\text{Si} + {}^{29}\text{Si} + 2\beta^- \ , \quad (13)$$

and

$$^{58}\text{Ti} \rightarrow 2{}^{29}\text{Si} + 6\beta^- \ . \quad (14)$$

The possibility of the production of lead starting from ^{197}Au-nH would not be neglected even if the isotopic composition of lead is close to the natural value. The transmutation reactions to produce heavier elements than gold would be endothermic. Hence, the production of mercury and lead indicates that both exothermic and endothermic processes are involved in the transmutation reactions that occurred in the present electrolysis. In heavy water electrolysis using palladium electrodes, we found the production of several elements heavier than palladium with anomalous isotopic compositions even for an electrode that exhibited no excess heat evolution.[12,13] Such a phenomenon would result in the compensation of the positive and negative heats caused by several exothermic and endothermic transmutation reactions. The possibility of this type of compensation effect was offered by Miley and Patterson[8] and Miley et al.[9]

The idea that elements heavier than tritium are involved directly in a cold nuclear reaction was first proposed by Bush.[17] He claimed to detect calcium and strontium in potassium carbonate and rubidium carbonate solutions, respectively, after light water electrolysis with nickel electrodes.[17,18] On the basis of these results, he proposed new types of fusion reactions involving alkali metal and hydrogen atoms. However, in the present study, an indication of the occurrence of the reaction $^{23}\text{Na} + \text{H} \rightarrow {}^{24}\text{Mg}$ was not obtained.

The concept that hydrogen atoms or protons interact with gold atoms to induce the aforementioned transmutation reactions is quite specific, but it is becoming current in the field of cold nuclear reaction. A trial of the theoretical interpretation of a nuclear transmutation reaction of this type has started.[19] Our results show that the manner of the occurrence of the nuclear transmutations depends on the electrolysis condition. In low current densities of <200 mA/cm^2, the product is exclusively iron. In current densities ranging from 300 to 750 mA/cm^2, mercury, krypton, nickel, and small amounts of various kinds of heavy metal elements are produced besides iron. In extremely high current densities >1 A/cm^2, silicon and magnesium are produced in addition to the preceding elements. Such characteristics of nuclear transmutation should be responsible for the concentration of hydrogen atom or proton and electrode potential. The hydrogen atom concentration is controlled by hydrogen overpotential. Therefore, electrode potential and hydrogen overpotential are major factors to control nuclear transmutation reactions.

It is known that a small fraction of extremely active hydrogen adsorbable sites, 0.03 to 0.04, occur on polycrystalline gold surfaces[20,21] on which the hydrogen evolution reaction occurs exclusively at a rate near that on platinum by a slow recombination mechanism.[22–24] This may mean that these sites are extraordinarily active for the hydrogen evolution reaction. Perhaps such sites are concentrated at the microcracks and holes, where lattice defects should be distributed at extremely high density. Therefore, it is expected that high hydrogen loading and an extremely strong electric field would be achieved at that place. The strong negative charge may further concentrate protons. In addition, it might be feasible that a small fraction of protons accepted electrons by the discharge under such a strong electric field happen to have a chance to convert into low kinetic energy neutrons:

$$\text{H}^+ + e \rightarrow n \ . \quad (15)$$

In such a circumstance, the conditions that could drive the aforementioned nuclear transmutation reactions could arise at any moment.

IV. SUMMARY AND CONCLUSIONS

In the present work we found the production of various kinds of elements with anomalous isotopic compositions on or in gold electrodes after electrolysis. The major elements were mercury, krypton, nickel, and iron. When electrolyzing at current densities of >200 mA/cm^2, fine porous precipitates were formed at the bottom of the electrolytic cell separated from the gold electrode. In the precipitates obtained at an extremely high current density, considerable amounts of silicon and magnesium with anomalous isotopic compositions were detected together with the aforementioned elements. The fact that a definite isotopic deviation occurred in several elements produced after the electrolysis indicates the occurrence of nuclear transmutations during the electrolysis.

In addition, a number of microcraters developed along the rim of the microcracks and microholes on the electrode surface during electrolysis. In view of the presence of hexagonal and rhombic crystallite layers on the inside wall of the craters, it is thought that very intense heat was produced in those places. The structure of the precipitates was very like that of the outside wall. This shows that the nuclear transmutation reactions took place in the cracks and holes, where the craters developed and the precipitates spewed out like volcanic ash. Therefore, lattice defects that should be concentrated at the cracks and holes are considered to play an important role in the nuclear transmutation reaction.

In electrolysis without extremely high current density, no anomalous elements lighter than iron were detected. Hence, we conclude that the nuclear transmutation reaction is initiated by the interaction between hydrogen atoms or protons and gold atoms of the electrode material. The production of mercury and lead shows that some endothermic processes may be involved in the transmutation reactions occurring in light water electrolysis with gold electrodes.

ACKNOWLEDGMENT

This study is supported by a grant-in-aid from the Thermal and Electric Energy Technology Foundation, Japan.

REFERENCES

1. T. OHMORI and M. ENYO, "Detection of Iron Atoms on Gold Used for Electrolysis of Neutral and Alkaline H_2O and D_2O Solutions," *Proc. Int. Symp. Cold Fusion and Advanced Energy Sources*, Minsk, Belarus, p. 218 (1994).

2. T. OHMORI and M. ENYO, "Iron Formation in Gold and Palladium Cathodes," *J. New Energy*, **1**, *1*, 15 (1996).

3. T. OHMORI, M. ENYO, T. MIZUNO, Y. NODASAKA, and H. MINAGAWA, "Transmutation in the Electrolysis of Light Water—Excess Energy and Iron Production in a Gold Electrode," *Fusion Technol.*, **31**, 210 (1997).

4. T. OHMORI, T. MIZUNO, H. MINAGAWA, and M. ENYO, "Low Temperature Nuclear Transmutation Forming Iron on/in Gold Electrode During Light Water Electrolysis," *Int. J. Hydrogen Energy*, **22**, 459 (1997).

5. T. OHMORI, T. MIZUNO, and M. ENYO, "Isotopic Distributions of Heavy Metal Elements Produced During the Light Water Electrolysis on Au Electrode," *J. New Energy*, **1**, *3* (1996).

6. T. OHMORI, T. MIZUNO, and M. ENYO, "Production of Heavy Metal Elements and the Anomalous Surface Structure of the Electrode Produced During the Light Water Electrolysis on Au Electrode," *Proc. 6th Int. Conf. Cold Fusion*, Toya, Hokkaido, Japan, 1996, Vol. 2, p. 670 (1996).

7. H. YAMADA, M. ISHIDA, Y. UMEZU, and H. HIRAHARA, "Products in the Light Water Electrolysis on Gold Cathode," *Proc. Solid State Nuclear Transmutation Symp.*, The Society of Material Engineering for Resources of Japan, Morioka, Japan, 1996, p. 93 (1997).

8. G. H. MILEY and J. A. PATTERSON, "Nuclear Transmutation in Thin-Film Nickel Coatings Undergoing Electrolysis," *Infinite Energy*, **2**, *9*, 19 (1996); see also *J. New Energy*, **1**, *3*, 1 (1996).

9. G. H. MILEY, G. NARNE, M. J. WILLIAMS, J. A. PATTERSON, J. A. NIX, D. CRAVENS, and H. HORA, "Experimental Observation of Massive Transmutations Occurring in Multilayer Thin-Film Microspheres After Electrolysis," *Proc. 6th Int. Conf. Cold Fusion*, Toya, Hokkaido, Japan, 1996, Vol. 2, p. 629 (1996).

10. J. DASH, G. NOBLE, and D. DIMAN, "Surface Morphology and Microcomposition of Palladium Cathodes After Electrolysis in Acidified Light and Heavy Water: Correlation with Excess Heat," *Trans. Fusion Technol.*, **26**, 299 (1994).

11. T. OHMORI, "Measurement of the Potential of Zero-Charge on Nickel Electrode by the Galvanostatic Transient Method," *J. Electroanal. Chem.*, **157**, 159 (1983).

12. T. MIZUNO, T. OHMORI, and M. ENYO, "Anomalous Isotopic Distribution in Palladium Cathode After Electrolysis," *J. New Energy*, **1**, *2*, 37 (1996).

13. T. MIZUNO et al., "Anomalous Isotopic Distribution of Elements Deposited on Palladium Induced by Cathodic Electrolysis," *Denkikagaku*, **64**, 1160 (1966).

14. H. NUMATA, R. TAKAGI, and I. OHNO, "Neutron Emission and Surface Observation During a Long-Term Evolution of Deuterium on Pd in 0.1 M LiOD," *Proc. Conf. Science of Cold Fusion*, Vol. 33, p. 71, T. BRESSANI, E. DEL GIUDICE, and G. PREPARATA, Eds., SIF, Bologna, Italy (1991).

15. T. MATSUMOTO, "Cold Fusion Experiments with Ordinary Water and Thin Nickel Foil," *Fusion Technol.*, **24**, 296 (1993).

16. A. C. MUELLER and B. M. SHERRILL, "Nuclei at the Limits of Particle Stability," *Ann. Rev. Nucl. Part. Sci.*, **43**, 529 (1993).

17. R. T. BUSH, "A Light Water Excess Heat Reaction Suggests That 'Cold Fusion' May Be 'Alkali-Hydrogen Fusion,' " *Fusion Technol.*, **22**, 301 (1992).

18. R. T. BUSH and R. D. EAGLETON, "Experiments Supporting the Transmission Resonance Model for Cold Fusion in Light Water: 1. Correlation of Isotopic and Elemental Evidence with Excess Heat," *Proc. 3rd Int. Conf. Cold Fusion*, Nagoya, Japan, 1992, p. 405 (1992).

19. Y. KUCHEROV, "Slow Nuclear Excitation Model," *Proc. 6th Int. Conf. Cold Fusion*, Toya, Hokkaido, Japan, 1996, Vol. 2, p. 502 (1996).

20. M. BREITER, C. A. KNORR, and W. VÖELKL, "Überspannungswerten auf Edelmetall-elektroden adsorbierten, mittels Ladekurven bestimmbaren wasserstoffmengen," *Z. Elektrochem. Ber. Bunsenges. Physik. Chem.*, **59**, 681 (1955).

21. F. G. WILL and C. A. KNORR, "Stromdichte-und pH-Abhängigkeit des elektrochemischen Auf- und Abbaus von Oxydshichten auf Pt, Pd und Au," *Z. Elektrochem. Ber. Bunsenges. Physik. Chem.*, **62**, 378 (1958).

22. T. OHMORI and M. ENYO, "Hydrogen Evolution Reaction on Gold Electrode in Alkaline Solutions," *Electrochim. Acta*, **37**, 2021 (1992).

23. S. SCHULDINER and J. P. HOARE, "An Electrochemical Study of Hydrogen Producing Reactions Catalyzed by Gold and Gold-Palladium Cathodes," *J. Phys. Chem.*, **61**, 705 (1957).

24. A. T. KUHN and M. BYRNE, "The Hydrogen- and Deuterium-Evolution Reaction on Gold in Acid Solutions," *Electrochim. Acta*, **16**, 391 (1971).

Tadayoshi Ohmori (BS, chemistry, Hokkaido University, Japan, 1962; Dr, electrochemistry, Hokkaido University, Japan, 1988) is currently a research associate at the Catalysis Research Center of Hokkaido University. His current research interests are interfacial energy conversion and characterization of active sites of the electrode.

Tadahiko Mizuno (BS, 1968; MS, 1970; and Dr, 1973, applied physics, Hokkaido University, Japan) is currently a research associate of the faculty of engineering at Hokkaido University. His current research interests are hydrogen storage material and localized corrosion.

Yoshinobu Nodasaka (BS, biography, Hokkaido University, Japan, 1969) is currently a member of the technical staff at the School of Dentistry of Hokkaido University. His current interest is the ultrastructure of materials.

Michio Enyo (BS, chemistry, Hokkaido University, Japan, 1953; PhD, electrochemistry, University of Pennsylvania, 1961) is currently president of the Hakodate National College of Technology. His current research interests are interfacial energy conversion and hydrogen electrosorption in metal.